The Origins and Future of Nuclear Magnetic Resonance Imaging

Felix W. Wehrli

Citation: Physics Today **45**, 6, 34 (1992); doi: 10.1063/1.881310
View online: https://doi.org/10.1063/1.881310
View Table of Contents: http://physicstoday.scitation.org/toc/pto/45/6
Published by the American Institute of Physics

THE ORIGINS AND FUTURE OF NUCLEAR MAGNETIC RESONANCE IMAGING

What began as a curiosity of physics has become the preeminent method of diagnostic medical imaging and may displace x-ray-based techniques in the 21st century.

Felix W. Wehrli

During the past two decades nuclear magnetic resonance has revolutionized chemistry, biochemistry, biology and, more recently, diagnostic medicine. Nuclear magnetic resonance imaging, or mri as it is commonly called, is fundamentally different from x-ray-based techniques in terms of the principles of spatial encoding and mechanisms of signal and contrast generation involved. Mri has a far richer ultimate potential than any other imaging technique known today, and its technology and applications are still far from maturation, which may not occur until early in the 21st century.

High-speed real-time mri eventually may guide the interventional radiologist and neurosurgeon and may permit imaging of brain function. In the latter application mri would be similar to positron emission tomography, but with the advantage that it would not require injection of imaging agents. Magnetic resonance imaging at microscopic dimensions will provide a new tool for visualizing minute anatomy and will permit nondestructive analysis *in vitro* and *in vivo*. Mri's ability to visualize blood flow already has led to magnetic resonance angiography, a new radiologic subspecialty that may supersede the invasive procedure of x-ray-based angiography, which requires injection of contrast material. Another emerging field is spectroscopic imaging, which will make possible image-guided biochemical analysis and thus the study of cellular metabolism *in vivo*.

This article reviews critically the major milestones in nuclear magnetic resonance's evolution from a curiosity of physics to an increasingly dominant technique for diagnostic medical imaging.

Felix Wehrli is a professor of radiologic science and director of magnetic resonance education at the University of Pennsylvania Medical Center, in Philadelphia.

Early history

Unbeknownst to the large majority of people who use magnetic resonance imaging, the history of this fascinating branch of science and technology has its roots in work performed well before World War II. In 1938 I. I. Rabi and his colleagues perfected a beam-splitting technique and successfully achieved nuclear magnetic resonance—a term that Rabi coined.[1] Their nmr experiments made use of the spin-state-dependent force that inhomogeneous magnetic fields exert on an atomic beam of silver atoms directed perpendicular to the gradient fields. For spin-$\frac{1}{2}$ nuclei the atomic beam splits, but it reconverges when the polarity of the gradient field reverses. Rabi showed that irradiating the spins at the transition frequency, which interchanges the $m = \pm \frac{1}{2}$ states, eliminated the convergence.

As remarkable as Rabi and his colleagues' experiment was, it was still a long way from present-day nmr, because it required an atomic beam, which can be generated only for a minority of materials. The first detection of nmr in bulk matter was achieved in the mid-1940s by research groups led by Edward M. Purcell at Harvard University and Felix Bloch at Stanford University.[2] Purcell used a resonant cavity to study the absorption of radiofrequency energy in paraffin; at resonance the cavity output was found to be slightly reduced. By contrast, Bloch and his colleagues used what they called "nuclear induction." Bloch described the experiment as measuring "an electromotive force resulting from the forced precession of the nuclear magnetization in the applied rf field."

When matter is placed in a magnetic field, the nuclear magnetic moments orient parallel to the field, leading to a

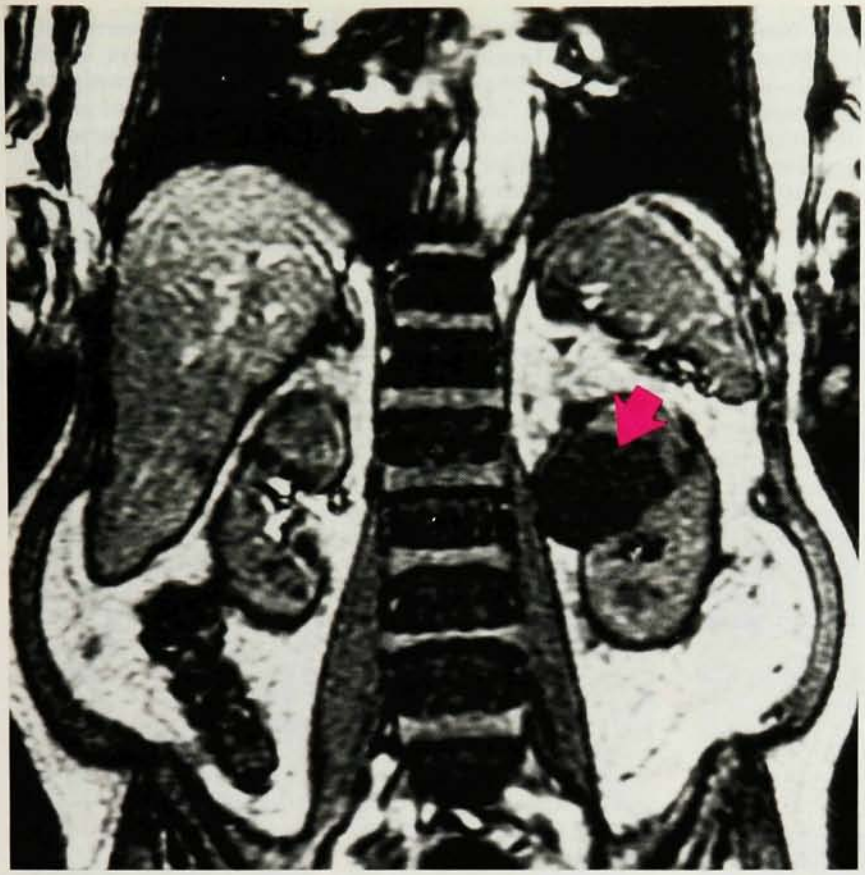

Magnetic resonance image of the abdomen. A large mass (arrow) in the left kidney shows up clearly. Advances in data acquisition technology have drastically reduced scan times: This image is one of 20 contiguous sections through the abdomen acquired in less than 1 minute using a high-speed imaging technique. **Figure 1**

paramagnetic polarization in the direction of the magnetic field—the z direction. If an oscillating magnetic field is applied in the x or y direction, the polarization vector is deflected from the z direction once the z field approaches the resonance value. The resonance condition is given by $|\gamma|B = \omega$, where B is the amplitude of the applied static magnetic field, ω is the nuclear precession frequency, and γ is the gyromagnetic ratio, which is a constant for a given isotope. In nmr, this rotation of the magnetic polarization vector of the nuclei in a plane perpendicular to the z axis induces an emf in a detector coil; this is the nmr signal.

Nuclear magnetic relaxation—that is, the return of the spin system to equilibrium—is of great significance to imaging and was conceptualized by these early investigators. By repeatedly passing the spin system through the resonance condition (by varying the amplitude of the polarizing magnetic field) and observing the reappearance of a signal, Bloch found that for protons (that is, hydrogen nuclei) in liquids the time constant T_1 for the return of the longitudinal magnetization was on the order of seconds. Further, he concluded from the sharpness of the resonance that the spins' phase memory time—the transverse relaxation time T_2—is on the order of hundreds of milliseconds in fluids (and, it would later turn out, only slightly shorter in biological tissues). It is clearly thanks to Mother Nature's good graces that nmr in human subjects is possible at all. If it took, instead of seconds, hours for the spins to repolarize, the technique would be impractical.

The commonly used detection method during the first two decades of nmr work exploited the principle of continuous-wave excitation, where the field is swept while the sample is irradiated with rf energy of constant frequency. An alternative scheme, which is still in use, consists of pulsed rf excitation followed by the detection of the resultant free-precession signal. Hence, rather than being simultaneous, in this scheme excitation and detection are performed sequentially.

A major milestone was the discovery of the chemical shift by Warren Proctor, F. C. Yu and W. C. Dickinson.[3] They found that in ammonium nitrate, two nitrogen-14 resonances could be observed, which they ascribed to the different chemical environments to which the nitrogen nucleus is exposed in the nitrate and ammonium ions. Similar findings were latter made by others for nuclei such as fluorine, phosphorus and hydrogen. These observations constitute the basis of modern nmr spectroscopy.

A few years later, as the magnetic field homogeneity, which determines the frequency resolution achievable in nmr, was improved further, another type of fine structure was discovered. This structure, which is due to spin–spin coupling, is fundamental to modern high-resolution spectroscopy, and together with the chemical shift provides the basic ingredients for molecular structure determination. Today nmr is the preeminent method for determining the structures of biomolecules with molecular masses up to 100 000 daltons.

An innovation without which modern nmr imaging would be inconceivable was the development of pulse Fourier-transform nmr by Richard Ernst and Weston Anderson.[4] This alternative mode of signal creation, detection and processing led to an unprecedented enhancement in per-unit-time detection sensitivity compared with continuous-wave excitation techniques. It is based on the Fellgett principle: If N channels are used simultaneously in an experiment, then, provided the dominant source of noise is not the excitation, the sensitivity increases by a factor $N^{1/2}$. Ernst and Anderson demonstrated that one can effect broadband excitation by exciting the nuclear spins with short rf pulses of a single

carrier frequency. Irving J. Lowe and Richard E. Norberg had previously shown that the response of the spin system to such pulses—the free-induction decay signal—is the Fourier transform of the absorption-mode spectrum.[5] In their seminal work, Ernst and Anderson demonstrated that in a typical proton nmr spectrum the signal-to-noise ratio per unit time can be improved by several orders of magnitude.

Imaging

A radically new dimension was added to nmr technology in 1973 when Paul Lauterbur at the State University of New York at Stony Brook first proposed generating spatial maps of spin distributions by what he called "nmr zeugmatography."[6] Key to this method was the idea of superimposing magnetic field gradients onto the main magnetic field to make the resonance frequency a function of the spatial origin of the signal. In the presence of a magnetic field gradient the frequency-domain signal is the equivalent of a projection of the object onto the gradient axis. By rotating the gradient (originally, the object) in small angular increments, one obtains a series of projections from which an image can be reconstructed using back-projection techniques.

These developments coincided in time with the pioneering work by Geoffrey Hounsfield at Hammersmith Hospital, London, whose application to x rays of the principle of filtered back-projection led to x-ray computed tomography.[7] Like CT, nmr zeugmatography used projection–reconstruction methods that were later superseded. (The later nmr technique is described in more detail below.) However, whereas CT evolved fairly rapidly into a clinical imaging technique, numerous technological hurdles had to be overcome before nmr could progress to clinical practicality.

By 1980 whole-body experimental nmr scanners were in operation, and by 1981 clinicians began to explore the clinical potential of magnetic resonance imaging. Nmr zeugmatography, as it still was called, had several advantageous properties not exhibited by x-ray CT. First, it was noninvasive—that is, it did not require ionizing radiation or the injection of contrast material. Second, it provided intrinsic contrast far superior to that of x-ray CT. (Figure 1 illustrates this contrast.) Some of this early work showed that magnetic resonance imaging was uniquely sensitive to diseases of the white matter of the brain, such as multiple sclerosis. Further, the contrast could be controlled to a significant extent by the nature and timing relationships of the radiofrequency pulses (now referred to as the rf pulse sequence)—a unique property of magnetic resonance imaging. Third, mri was truly multiplanar and even three dimensional—that is, it could provide images in other than the traditional transverse plane without the subject having to be repositioned. This property rapidly turned out to be invaluable and a significant advantage over x-ray CT for the study of the brain and other organs.

The spatial encoding process

In 1975 Ernst introduced a new class of nmr experiments, now commonly referred to as two-dimensional nmr.[8] The significance of this development, which laid the groundwork for structural and conformational analysis of large biological macromolecules, was highlighted when Ernst was awarded the 1991 Nobel Prize in chemistry (see PHYSICS TODAY, December 1991, page 19).

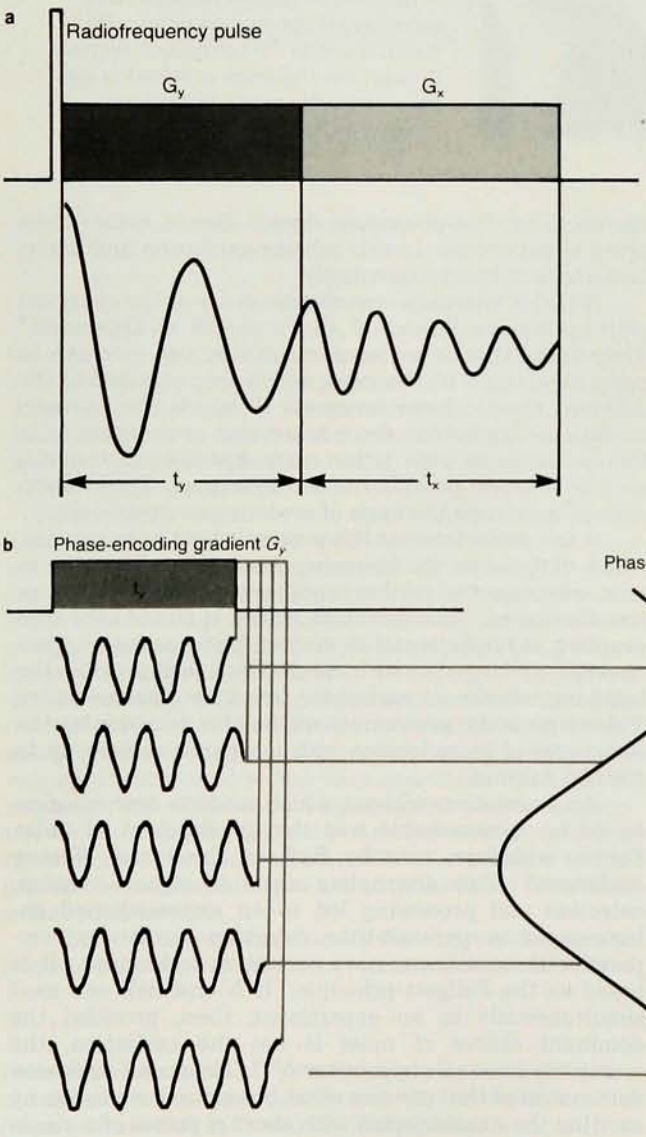

Fourier zeugmatography principle. **a:** A point source of spin density $\rho(x,y)$ is alternately exposed to magnetic field gradients G_x and G_y. Following excitation, the spins first precess during a period t_y in the presence of a magnetic field gradient of amplitude G_y at a frequency ω_y proportional to their spatial position y and to the gradient amplitude: $\omega_y = \gamma G_y y$, where γ is the gyromagnetic ratio. Thereafter an orthogonal gradient is activated and the spins precess at a second frequency ω_x, which is proportional to their spatial position x and to the gradient amplitude G_x—that is, $\omega_x = \gamma G_x x$. The signal is detected during this period. **b:** Stepping the duration (or amplitude) of the gradient G_y causes the phase of the transverse magnetization to change cyclically. The signal's phase is related to its y location; its frequency, to its x location. **Figure 2**

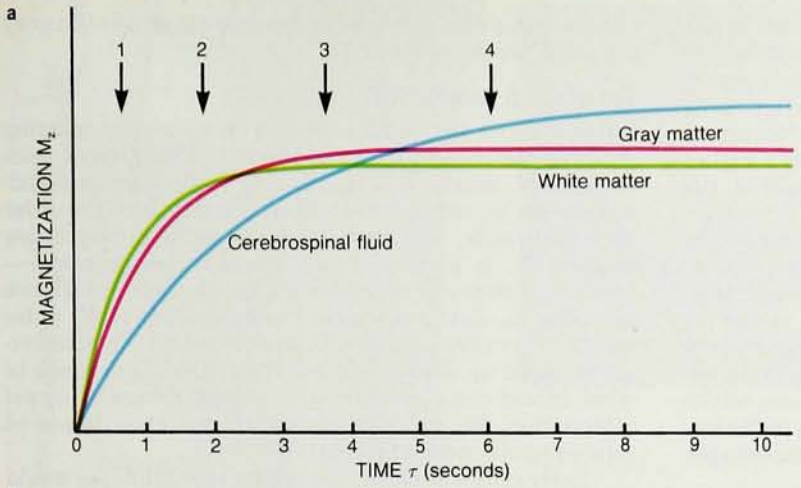

Contrast continuum. **a:** Evolution of the longitudinal magnetization for protons in white matter, gray matter and cerebrospinal fluid. The relaxation times T_1 usually follow a single-exponential rate law. **b:** Images of the brain corresponding to the pulse-recycle times indicated in **a** exhibit differing contrast. **Figure 3**

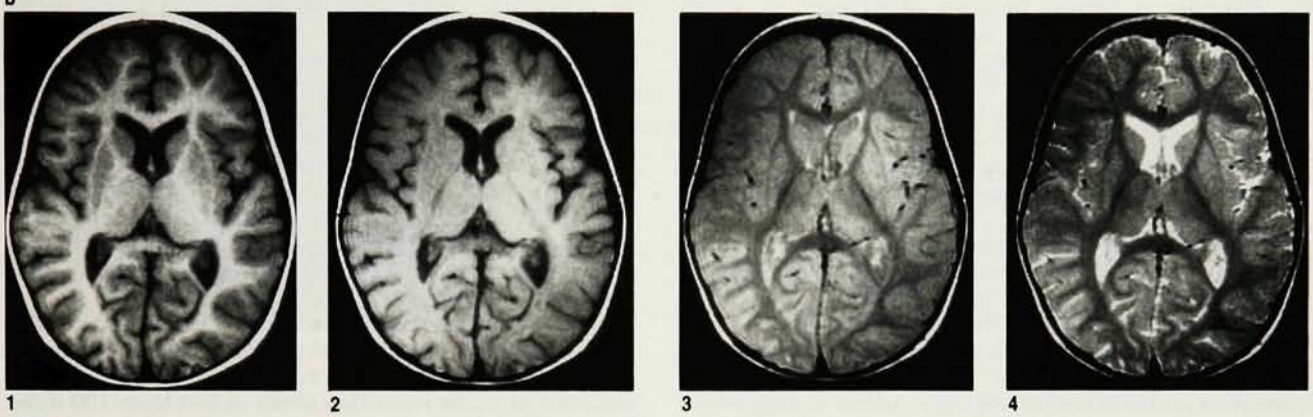

A *one*-dimensional nmr spectrum is a plot of the amount of energy absorbed versus the resonance frequency, the latter being determined by the spins' chemical shift and spin–spin coupling. Suppose in the molecule under investigation each hydrogen is spin-coupled to a carbon nucleus. A specific example of a *two*-dimensional spectrum would then be a plot of carbon-13 signal amplitude versus both carbon-13 and proton resonance frequency. Hence the spectrum has the characteristics of a surface. Examination of this spectrum permits one to determine immediately which pairs of nuclei are coupled to each other and thus are spatial neighbors.

Like the two-dimensional spectrum, an image may be regarded as a two-dimensional array of signal amplitude versus two spatial coordinates, say x and y. Almost concurrent with his general description of two-dimensional nmr, Ernst demonstrated an embodiment of this idea designed to map a spatial distribution of spins. The experiment, which was called "nmr Fourier zeugmatography," should be regarded as the parent of many modern mri techniques.[9]

One can understand the principle by reference to figure 2a. Suppose the spins in a point object of spin density $\rho(x,y)$ are excited by an rf pulse in the presence of a magnetic field gradient of amplitude G_y, which we call a phase-encoding gradient. These spins will resonate at a relative frequency $\omega = \gamma B(y)$, where $B(y) = G_y y$. If the gradient is active for a period t_y, the phase at the end of the gradient period is $\phi_y = \gamma G_y y t_y$. Let us then step the time t_y in equal increments, as implied by figure 2b. We readily notice that the phase at the end of the gradient period varies cyclically with time. At time $t = t_y$, the gradient G_y is turned off and an orthogonal gradient G_x is applied for a duration t_x, during which the free-induction decay signal is collected. During the detection period the spins precess at a frequency $\omega_x = \gamma G_x x$. One thus encodes spatial information into both the phase and the frequency of the nmr signal, whose amplitude is proportional to $\rho(x,y)$. Of course, in the case of imaging a real object, the signal has a multitude of frequency and phase components.

An obvious drawback of stepping the duration of the gradient G_y is the decrease in signal amplitude due to the irreversible decay (with relaxation time T_2) of the transverse magnetization. Because the phase shift imparted to the signal by the gradient G_y is a function of the gradient's duration as well as its amplitude, one can achieve the same effect by stepping the amplitude of the gradient while keeping its duration constant. This important modification of the technique gave rise to what is called spin-warp imaging.[10] The term refers to the "warping" of the phase caused by the gradient. Raising the amplitude of the first gradient incrementally during each excitation-and-read cycle yields an $N_1 \times N_2$ array of raw data, from which one can reconstruct an image by double Fourier transformation of the signal. The resulting digital image consists of $N_1 \times N_2$ picture elements, or pixels, whose values are proportional to the amplitudes of the detected transverse magnetizations. The process of incrementally increasing a gradient in amplitude to encode spatial information into the phases of precessing spins is called phase encoding.

Spin relaxation and nmr gray scale

Perhaps the most salient feature of nmr relative to x-ray-based techniques such as CT is the extraordinarily large innate contrast, which can be on the order of several hundred percent for adjacent soft tissues. In x-ray imaging, contrast is a consequence of differences in the

attenuation coefficients of adjacent structures and is on the order of a few percent at best. Attenuation coefficients are related to electron densities, which are roughly proportional to the atomic numbers of the elements present. Thus fat, being rich in carbon, is more "transparent" to x rays than is water, because oxygen has a higher atomic number than carbon. This is the basis of the Hounsfield-number scale.

The basis of the signal and contrast in nmr is the transient nature of the signal. Spins, following excitation, return to their equilibrium state with characteristic time constants, the spin relaxation times T_1 and T_2, which for water in biological tissues are on the order of hundreds of milliseconds or even seconds. This process can be described by the phenomenological Bloch equations, which predict the evolution of the spin system in terms of the longitudinal and transverse components of the complex spin magnetization.

Consider a typical imaging experiment in which radiofrequency pulses are applied repeatedly at time intervals $\tau < T_1$ for the purpose of spatial encoding. Then the magnetization available for detection is attenuated by a factor $1 - e^{-\tau/T_1}$. This, in itself, would not be a sufficient mechanism for modulating the image signal were it not for the large range of relaxation times found for the water protons in mammalian tissues—from about 100 msec to several seconds.

Though the process of tissue water relaxation is not completely understood, its rate is related to the extent of binding of water to the surface of biological macromolecules. Increased binding slows molecular motion. The more closely the reorientational motion of the magnetic dipoles matches the Larmor frequency, the greater the transition probabilities between the nuclear energy levels, and thus the greater the relaxation rates. A case in point is the brain, the majority of which consists of gray and white matter adjacent to fluid-filled cavities, the ventricles. Because water is more tightly bound in white matter than in gray mater, the water molecules in white matter reorient more slowly than those in gray matter, thus more closely matching the Larmor frequency; hence $T_{1,wm}$ is less than $T_{1,gm}$. By contrast, spinal fluid, which from the point of view of molecular motion closely parallels neat water, has much faster molecular motion, and thus $T_{1,sf}$ is much greater than both $T_{1,wm}$ and $T_{1,gm}$.

The evolution of the longitudinal magnetization for the three types of protons is shown in figure 3a. The equilibrium magnetization is proportional to the proton concentration in the tissue, hence the different plateau values. For short pulse-recycle times ($\tau \ll T_1$) the signal amplitudes follow the reciprocal of T_1, whereas at long recycle times ($\tau \gg T_1$) they are governed by their equilibrium magnetization—that is, they follow the proton concentrations. This is borne out by the images in figure 3b, which correspond to the τ values labeled 1–4 in figure 3a. Contrast in mri is therefore a continuum, and unlike in x-ray imaging, there is no universal gray scale.[11] Further, it was recognized early on that in most diseased tissues, such as tumors, the relaxation times are prolonged.[12] This difference provides the basis for image contrast between normal and pathological tissues.

The foregoing assumes that the transverse magnetization observed is equal to the longitudinal magnetization prior to excitation—that is, that data sampling immediately follows creation of the signal. If, by contrast, the signal readout is delayed, the transverse magnetization is attenuated by a factor $\exp(-\Delta/T_2)$, where Δ is the readout delay and T_2 is the transverse relaxation time. Like T_1, T_2 in biological tissues covers a large range—from about 50 to 500 msec. Hence, by delaying the readout of the signal, one can get a different type of contrast for which the gray scale follows the order of T_2.

Temporal resolution

We saw above that data sampling in spin-warp imaging requires the collection of N_y free-induction decays, each sampled N_x times. Whereas during the frequency-encoding process N_x samples are acquired in a time on the order of milliseconds, the time interval between successive samples N_y is at least one pulse repetition period τ—typically hundreds of milliseconds, or seconds. Hence sampling N_y data rows takes the equivalent of N_y pulse repetition periods, which is usually minutes. In attempting to speed up data collection, the critical question is to what extent one can shorten τ without excessive signal attenuation due to spin saturation and thus impaired signal-to-noise ratio and contrast.

Early critics of mri asserted that the technique would be inherently slower than its x-ray-based counterparts: The duration of T_1 relaxation times, being on the order of hundreds of milliseconds up to seconds, would be a major physical barrier to reaching data acquisition rates anywhere near those of x-ray CT. This misconception was the result of a major oversight in the nmr literature. Until 1985 virtually all imaging experiments were based on 90° rotation of the spin magnetization by the rf excitation—so-called 90° pulses. But in their seminal paper on pulse Fourier-transform spectroscopy, Ernst and Anderson had shown[4] that the optimal excitation angle is considerably less than 90° whenever $\tau < T_1$.

In 1986 Axel Haase and Jens Frahm at the Max Planck Institute for Biophysical Chemistry in Göttingen, Germany, first reported[13] magnetic resonance images obtained at pulse repetition times of less than 100 msec. These rates afforded imaging times on the order of a few seconds rather than minutes. More recently, owing to advances in scanner hardware (gradient and rf subsystems), pulse repetition times of less than 10 msec have become possible, reducing total image acquisition time to 1 second or less.

One significant difficulty in mri has been physiological motion such as that arising from breathing or the beating of the heart. Motion, besides causing blur, has various other adverse manifestations. In rectilinear sampling, such as spin-warp imaging, periodic motion causes an amplitude or phase modulation of the magnetic resonance signal, which leads to ghost artifacts in the images. One frequently practiced remedy is to synchronize the data acquisition with the cardiac cycle—so-called cardiac gating.

If the total data acquisition time could be made less than the period of such motion, artifacts could be significantly reduced. Although a total data sampling time on the order of 1 second does not seem to satisfy this requirement, it turns out that only a fraction of the data need be sampled in a time short relative to the period of motion. Indeed, as long as the fraction of data space containing the low spatial frequencies is sampled in a small portion of the period of motion, artifacts are largely eliminated. Figure 1 is a coronal image of the abdomen showing a large lesion in a kidney, obtained with a high-speed gradient-echo imaging technique. In this case images corresponding to 20 contiguous sections covering the entire abdomen were scanned in less than 1 minute.

One can augment the scan rate further by collecting many lines of data from the response to a single excitation. To do this one can generate, from a single rf excitation, a train of echoes, each of which is separately encoded. If the sampling rate is sufficiently fast, the entire data space can be mapped during a single read cycle. Because the signal's

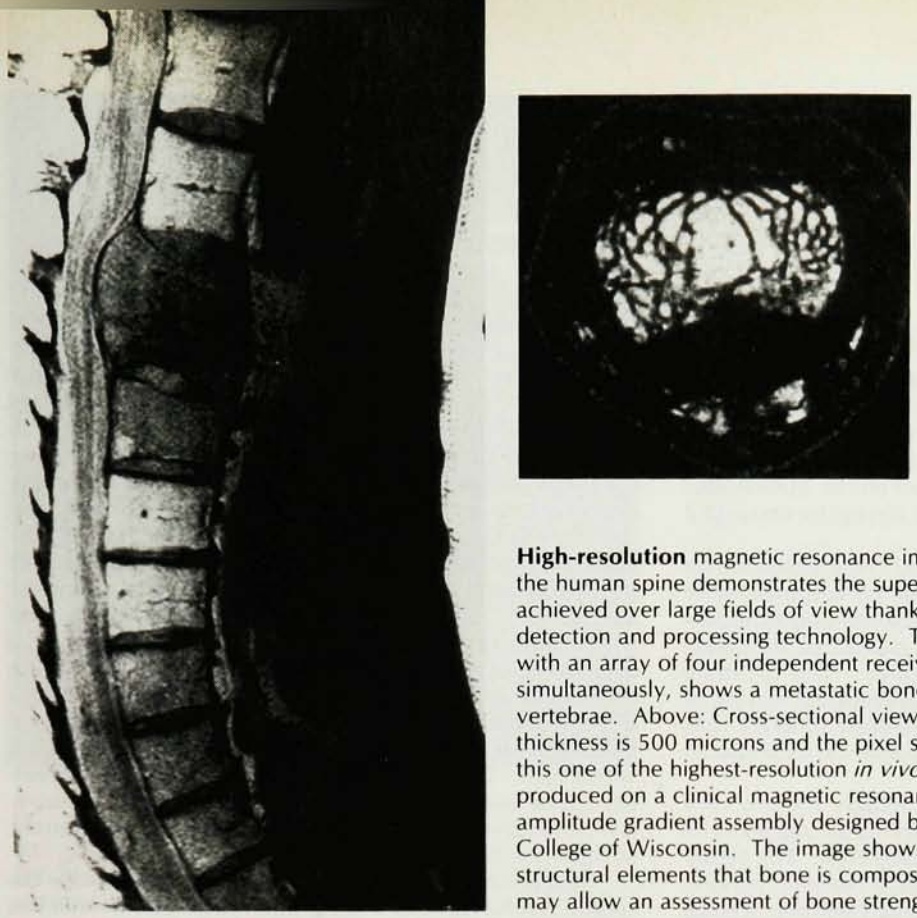

High-resolution magnetic resonance images. Left: Sagittal image of the human spine demonstrates the superb resolution that can be achieved over large fields of view thanks to improvements in rf detection and processing technology. This image, which was collected with an array of four independent receiving coils operating simultaneously, shows a metastatic bone tumor involving two vertebrae. Above: Cross-sectional view of the middle finger. The slice thickness is 500 microns and the pixel size is 78×78 microns, making this one of the highest-resolution *in vivo* images ever obtained. It was produced on a clinical magnetic resonance imager using a high-amplitude gradient assembly designed by Eric Wong at the Medical College of Wisconsin. The image shows individual trabeculae—the structural elements that bone is composed of—an analysis of which may allow an assessment of bone strength. **Figure 4**

lifetime is on the order of T_2, the total sampling period cannot exceed T_2, which in practice is about 50–200 msec. Such a scheme, first devised by Peter Mansfield, is known as echoplanar imaging.[14] The advent of instrumentation equipped with low-inductance gradient coils and powerful amplifiers now permits collection of an entire raw data set in 50 msec or less.[15]

Using contrast material in conjunction with these techniques makes it possible to measure the transit time of blood across the brain and other organs to assess organ perfusion. While mri, thanks to its outstanding contrast and spatial resolution, is already the undisputed leader in morphological imaging, we are currently witnessing a transition from morphological and anatomical to functional imaging. Recently it was shown that one can use the technology outlined above to map brain function in a manner similar to positron emission tomography. Jack Belliveau and his colleagues at Massachusetts General Hospital measured the change in regional cerebral blood volume in response to photic stimulation.[16] These experiments were based on a combination of injection of contrast material and subtraction of a series of images acquired at temporal increments of 750 msec, with and without application of a stimulus.

Speeding up the reconstruction process will make true real-time imaging accessible in the near future. Magnetic resonance imaging might then be used in a manner analogous to ultrasound. The prospects of performing interventional procedures, guided by mri, in the magnet therefore do not seem to be farfetched. Other applications being targeted are in cardiovascular imaging, where current methods are hampered by arrhythmia, which prevents the use of cardiac gating.

Spatial resolution

Although not identical with spatial resolution, a useful figure of merit is pixel size. Improvement of spatial resolution, as in any digital imaging technique, requires sampling the higher spatial frequencies. In mri, the spatial frequency is proportional to the amplitude of the imaging gradients and to their duration. Increasing the duration means increasing the sampling time, and there are obvious limits to doing this, not least among them the finite duration of the signal. Because the power requirements of the gradient amplifiers increase roughly as the fifth power of the coil diameter, there are practical limits to achieving gradient amplitudes for whole-body gradient coils much in excess of 1–2 gauss/cm. However, it is relatively straightforward to increase gradient amplitudes to 100 gauss/cm or more for imaging objects of a centimeter or less. The currently proven[17] resolution in the small-object domain—often called the domain of nmr microscopy—is on the order of 5–10 microns.

The smallest signal-producing entity in a digital image is the volume element, or voxel, and thus the signal-to-noise ratio scales with voxel size. Assuming equal resolution in all three orthogonal directions, the signal-to-noise ratio thus is proportional to the cube of the pixel size, $(\Delta r)^3$. Hence, to lower the pixel size by two orders of magnitude, say from 1 mm to 10 microns, would require a millionfold increase in the signal-to-noise ratio! Because the signal-to-noise ratio also scales with sampling time, some of the signal-to-noise ratio loss can, in principle, be offset by signal averaging. However, the signal-to-noise ratio scales only as the square root of the total sampling time, so this approach is clearly impractical. In practice, the only viable strategy is to lower the physical dimensions of the imaging volume, permitting the use of small receiver coils, which are inherently more efficient.

A further means of enhancing detection sensitivity is to increase the magnetic field. For human-sized lossy samples, the noise of the receiver circuit is governed by sample resistance, and therefore the signal-to-noise ratio increases only linearly with the field strength. Further,

equipment cost and siting constraints limit the field strength to about 2 tesla for whole-body imagers. In the small-sample limit, by contrast, the receiver coil is the dominant source of resistance. Under these conditions the signal-to-noise ratio scales as the $^7/_4$ power of the magnetic field, and so the potential gains from increased field strength are significant. Thus small-object microscopic imaging has been conducted at field strengths up to 11.7 tesla.

However, even if the technical requirements for achieving a pixel size of 100 microns, for example, were met in terms of both gradient amplitudes and signal-to-noise ratio, there would still be no guarantee that such resolution would actually be attained. The ultimate constraint is usually motion, be it physiological motion or motion of the entire subject. It is therefore unlikely that spatial resolutions of 50 microns can ever be exceeded *in vivo* in humans.

Figure 4 shows high-resolution images for two very different clinical applications. The first is an image of the spine obtained with an array of surface coils. The signal from each coil was fed to an independent receiver, making it possible to optimize the signal-to-noise ratio over a large field of view. The second image is a cross-sectional view of the middle finger displaying the individual trabeculae, the structural elements that give bone its mechanical strength.

Imaging of flow

Magnetic resonance imaging is extraordinarily sensitive to flow. Two distinct effects account for this high sensitivity. First, nmr images are typically recorded under conditions of partial saturation of the spins. In this regime the spins are excited repeatedly, as described previously, at intervals $\tau < T_1$, and hence return a signal that is substantially attenuated. Assuming the rf stimulation occurs by means of 90° pulses, the resultant tissue signal is reduced by a factor $1 - \exp(-\tau/T_1)$, which for $\tau = 50$ msec and a tissue time constant T_1 of about 1 second, for example, corresponds to a 95% signal reduction. By contrast, blood entering the imaging volume between successive excitations carries the full magnetization and thus appears enhanced relative to the stationary tissue protons—by a factor of about 20 in the example just given. Hence, in a stack of thin-section images perpendicular to the direction of the flow, vessels appear with high intensity and the stationary background is virtually suppressed. By reprojecting such a data set, one can obtain a vascular projection image, or angiogram. The reprojection algorithm entails casting parallel rays in the projection direction. By retaining only the highest-intensity pixel that each ray encounters on its projection path, one can significantly reduce the background signal. Vascular structures, which have 10–20-fold higher signal amplitudes than their stationary counterparts, are highlighted.

The second effect exploited for generating vascular images is the phase change that the transverse magnetization of moving spins experiences relative to that of their stationary counterparts. To understand this effect, suppose first that stationary spins at location r are exposed to a magnetic field gradient G. These spins accumulate a relative phase $\phi = \omega t = \gamma G r t$. By contrast, spins moving at some velocity v will sense a linearly increasing frequency $\omega = \gamma G(r + vt)$ and thus accumulate phase faster: $\phi = \gamma G(rt + vt^2/2)$. Hence, moving spins can be recognized on the basis of the extra phase shift they experience. In practice, one achieves this discrimination by acquiring two data sets—for example, one with and one without application of a flow-encoding gradient. Complex subtraction of the two data sets then affords an image free of the stationary background signal and displaying vascular structures only. This technique, known as phase-contrast angiography, is used to visualize relatively slow flow, where the inflow angiography described above fails because of saturation of the blood signal.[18] Figure 5, a phase-contrast projection magnetic resonance angiogram of the vessels of the brain, reveals a small aneurysm—a bulging of an artery resulting from local weakening of the vessel wall. This abnormality, if undetected and untreated, can be fatal. Because magnetic resonance is noninvasive, it lends itself as a screening technique for populations at high risk of such disorders.

Magnetic resonance angiography does not provide the spatial resolution of its x-ray counterpart. However, it has certain significant advantages. First, it requires neither injection of contrast material nor imposition of a radiation hazard. Second, from a single data set, images can be reconstructed at arbitrary projection angles, allowing the physician to visualize the vascular tree from many directions. Widespread clinical use of magnetic resonance angiography is currently hampered by the limited availability of magnetic resonance devices. Also, at the current state of the art, magnetic resonance angiography is plagued by signal-loss artifacts resulting from complex flow. But these problems will certainly be overcome, and we are likely to witness a steady decline of conventional angiography during this decade in favor of procedures based on magnetic resonance.

Metabolic imaging

In the 1970s nmr spectroscopy was already a highly developed discipline, and its extension to the study of live tissue as a means for obtaining metabolic information appears, in hindsight at least, to have been rather straightforward. In 1973 high-resolution ^{31}P nmr spectra of intact red blood cells were reported from which individual phosphorus metabolites could be identified; subsequently, the same was done for intact muscle.[19] The idea of sampling the signal from a small volume of tissue by means of what we now call the surface coil made spectroscopic nmr possible in live animals and ultimately humans. Britton Chance at the University of Pennsylvania and George Radda at Oxford University have made extensive use of ^{31}P nmr to study cellular metabolism *in vivo*.[20]

In an nmr spectrum, resonance absorption is measured as a function of frequency, with the frequency dispersion being caused by the chemical shift. An added complication of spectroscopy on human subjects is the requirement for some form of localization. By encoding spatial information into the phase of the rf signal by modulating either the static or the rf field, one can reconcile the principles of imaging and spectroscopy. This

Magnetic resonance angiogram showing the left carotid artery and middle cerebral artery in the brain. The latter supplies blood to part of the left hemisphere of the brain. This image, which was obtained by the phase-contrast technique, reveals a small aneurysm about 5 mm in diameter (arrow)—a bulging of the vessel caused by local weakening of the vessel wall. Such an abnormality is potentially life threatening. **Figure 5**

approach proved to be a means of imaging chemically shifted species.[21] Instead of reading the signal in the presence of a frequency-encoding gradient, which would provide additional frequency dispersion, one collects the signal in the absence of any gradient. The result, following the usual double Fourier transformation, is a map of spatial spin density versus chemical shift. Chemical-shift imaging can be extended to all three spatial coordinates, so that a three-dimensional data array can be created in which each element represents a spatially localized spectrum.

The medical applications of chemical-shift imaging are almost unlimited. First, it can be implemented for any nucleus of sufficient chemical and isotopic abundance—on the condition, of course, that there is more than one chemically shifted constituent. Prime candidates, however, are hydrogen, phosphorus-31 and carbon-13. Figure 6a shows a proton image in a patient with a malignant brain tumor, and figures 6b–d show regional spectra in the same patient.[22] Note that the neurochemical *N*-acetyl aspartate is not present in the tumor, and the choline level is elevated—both characteristics of rapidly proliferating cells.

A significant limitation of chemical-shift imaging—compared with positron emission tomography, for example—is its detection sensitivity. Most of the metabolites of interest are present at only millimolar concentrations, as opposed to cellular water, which has a concentration of about 40 moles/liter. Hence the intrinsic signal-to-noise ratio in metabolic imaging is reduced by a factor of 10^4 relative to tissue water. This loss can be offset in practically only one way—by trading spatial resolution for sensitivity. Remembering that the signal-to-noise ratio is proportional to the voxel size, and assuming a typical lower limit of about 10^{-4} cm^3 for bulk proton imaging, this translates into typical voxel sizes for chemical-shift imaging on the order of about 1 cm^3, consistent with a linear resolution of about 1 cm.

Long-term outlook

We can only speculate on forthcoming innovations beyond the next few years, but it is likely that mri will continue to evolve well into the 21st century. One of the conceivable applications of real-time ultrafast imaging is whole-body screening of high-risk populations, possibly enabling detection of disease well before it becomes symptomatic. Clearly, the enormous impetus this application would give mri could result in hundreds of millions of examinations per year. Examination times are likely to approach a few minutes per patient within the next 5–10 years. This advance will be achieved by incorporating and perfecting high-speed imaging techniques along with improving the efficiency of the imager's patient and operator interfaces.

The prospect of mri's eventually even displacing chest-film radiography seems farfetched yet not unrealistic. The technology for rapid tomographic imaging of the entire torso in seconds is clearly on the horizon. While the equipment cost for such instrumentation exceeds that of a chest x-ray machine by an order of magnitude, this may not necessarily be an impediment, for two reasons. First, mri has already been shown to provide vastly superior information. Second, rather than instrument cost, the relevant criterion is the cost per procedure, which, with the anticipated speed enhancements, may become competitive for mri. Because of the massive amount of data that will be generated if this change comes about, computer-aided image analysis by means of expert systems, with minimal human intervention, will likely take the place of conventional image interpretation.

The emergence of new superconducting materials with higher current-carrying capacity will lead to magnets with fields well beyond the current limits. Already, using conventional superconducting materials, whole-body nmr magnets have been constructed[23] that operate at field strengths up to 4 tesla, and the design of such magnets with field strengths up to 10 tesla using niobium–tin superconductors appears to be within the reach of current technology, albeit at a cost that will limit their diffusion. The increase in the signal-to-noise ratio brought about by the higher magnetic fields should make it possible to perform chemical-shift imaging at much improved spatial resolution on such biological nuclei as carbon-13, sodium-23, phosphorus-31, potassium-39 and deuterium.

Magnetic resonance imaging does have inherent

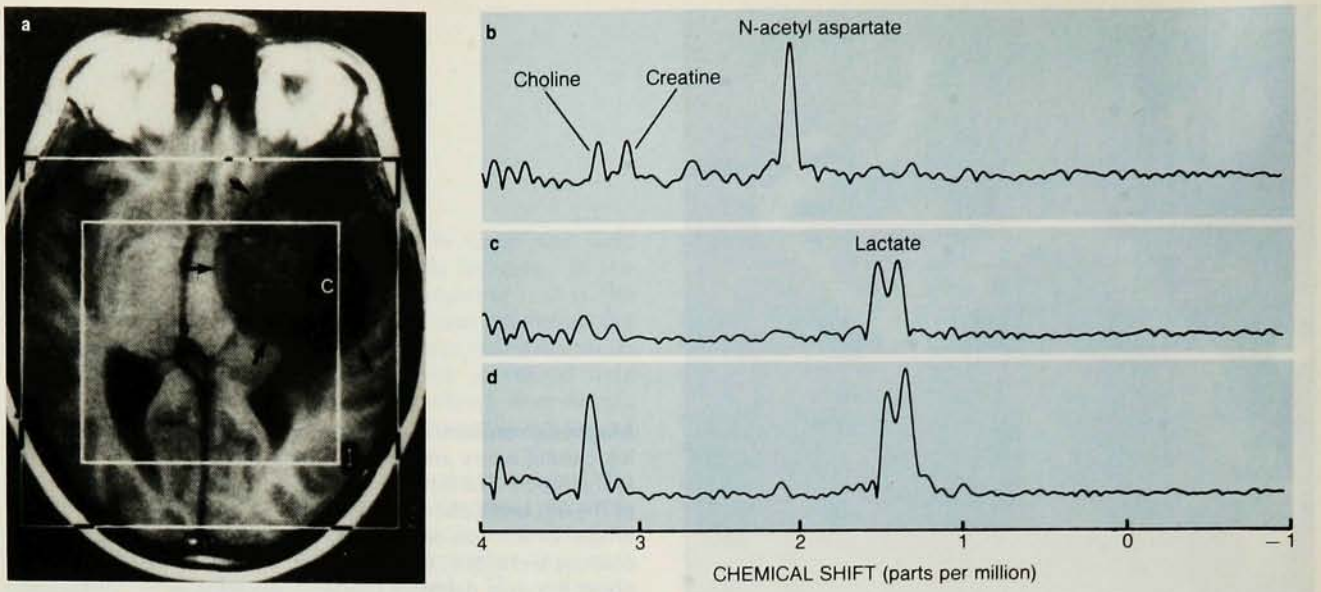

Malignant brain tumor and proton spectra of various regions. **a:** Magnetic resonance image; arrows indicate extent of tumor. The inner box represents the boundaries of the volume selected for spectroscopic imaging. A defect due to surgery is marked C. The three regional nmr spectra **b–d** show resonance absorption as a function of chemical shift (in parts per million of resonance frequency) for several brain metabolites. Each spectral peak corresponds to a specific metabolite, as indicated. **b:** Control region corresponding to normal brain. **c:** Region of postsurgical defect. **d:** Solid region of tumor. Note that in the tumor, *N*-acetyl aspartate is absent and choline is elevated. (Adapted from ref. 22.) **Figure 6**

limitations. Compared with x-ray- and radionuclide-based techniques, nmr is relatively insensitive. Hence any substantial future enhancement of the technology will hinge on our ability to improve detection sensitivity. Unfortunately the prospects for more than incremental gains in sensitivity are relatively bleak. A quantum leap in detection sensitivity is theoretically possible through the technique of "electron–nuclear double resonance," which takes advantage of the fact that electron spins are coupled to nuclear spins by a dipolar mechanism. Irradiation at the electron spin resonance frequency during detection of the nuclear magnetic resonance induces an electron–nuclear Overhauser effect—an enhancement that increases the nmr signal several-hundred-fold.[24] The exploitation of this effect for selective local signal enhancement, first proposed in 1980 by Raymond Andrew at Nottingham University in England, was recently reported: Injection of a targetable paramagnetic molecule made it possible for irradiation at the electron spin resonance frequency to cause such enhancement. This technique may enable diagnosis of early malignancies before they can be detected by conventional means, thus providing a tool for screening high-risk populations.

Magnetic resonance imaging is likely to emerge as the universal mode of medical imaging of the 21st century, possibly displacing x-ray-based techniques. Whether or not this happens will depend on the procedure's cost effectiveness relative to competing techniques such as ultrasound.

References

1. I. I. Rabi, J. R. Zacharias, S. Millman, P. Kusch, Phys. Rev. **53**, 318 (1938).
2. E. M. Purcell, H. C. Torrey, R. V. Pound, Phys. Rev. **69**, 37 (1946). F. Bloch, W. W. Hansen, M. Packard, Phys. Rev. **70**, 474 (1946).
3. W. G. Proctor, F. C. Yu, Phys. Rev. **77**, 717 (1950). W. C. Dickinson, Phys. Rev. **77**, 736 (1950).
4. R. R. Ernst, W. A. Anderson, Rev. Sci. Instrum. **37**, 93 (1966).
5. I. J. Lowe, R. E. Norberg, Phys. Rev. **107**, 46 (1957).
6. P. C. Lauterbur, Nature **243**, 190 (1973).
7. G. N. Hounsfield, Br. J. Radiol. **46**, 1016 (1973).
8. L. Müller, A. Kumar, R. R. Ernst, J. Chem. Phys. **63**, 5490 (1975).
9. A. Kumar, D. Welti, R. Ernst, J. Magn. Res. **18**, 69 (1975).
10. W. A. Edelstein, J. M. S. Hutchison, G. Johnson, T. Redpath, Phys. Med. Biol. **25**, 751 (1980).
11. F. W. Wehrli, J. R. MacFall, G. H. Glover, G. N. Grigsby, V. Haughton, J. Johanson, Magn. Res. Imaging **2**, 3 (1984). I. R. Young, Br. Med. Bull. **40**, 139 (1984).
12. R. Damadian, Science **171**, 1151 (1971).
13. A. Haase, J. Frahm, D. Matthaei, J. Magn. Res. **67**, 258 (1986).
14. P. Mansfield, J. Phys. C **10**, 55 (1977).
15. M. S. Cohen, R. M. Weisskoff, Magn. Res. Imaging **9**, 1 (1991).
16. J. W. Belliveau, D. N. Kennedy, R. C. McKinstry, B. R. Buchbinder, R. M. Weisskoff, M. S. Cohen, J. M. Vevea, T. J. Brady, B. R. Rosen, Science **254**, 716 (1991).
17. Z. H. Cho, C. B. Ahn, S. C. Juh, H. K. Lee, Med. Phys. **15**, 815 (1988). G. P. Cofer, J. M. Brown, G. A. Johnson, J. Magn. Res. **83**, 608 (1989).
18. C. L. Dumoulin, S. P. Souza, M. F. Walker, W. Wagle, Magn. Res. Med. **9**, 139 (1989).
19. R. B. Moon, J. D. Richards, J. Biol. Chem. **248**, 7276 (1973). D. I. Hoult, Nature **252**, 285 (1974).
20. For a review, see P. A. Bottomley, Radiology **170**, 1 (1989).
21. J. Cox, P. J. Styles, J. Magn. Res. **40**, 209 (1980). T. R. Brown, P. M. Kincaid, K. Ugurbil, Proc. Natl. Acad. Sci. USA **79**, 3523 (1982).
22. P. R. Luyten, A. J. H. Marien, W. Heindel, P. H. J. van Derwen, K. Herholz, J. A. van Hollander, G. Friedmann, W.-D. Heiss, Radiology **176**, 791 (1990).
23. H. Barfuss, H. Fischer, D. Hentschel, R. Ladebeck, J. Vetter, Radiology **169**, 811 (1988). C. J. Hardy, P. A. Bottomley, P. B. Roemer, R. Redington, Magn. Res. Med. **8**, 104 (1988).
24. A. W. Overhauser, Phys. Rev. **92**, 411 (1953). ■